Desalination and Water Treatment
www.deswater.com
doi: 10.1080/19443994.2015.1012748

57 (2016) 7054–7065
March

Taylor & Francis
Taylor & Francis Group

Removal of anionic dyes from aqueous solution by adsorption onto amino-functionalized magnetic nanoadsorbent

Zhijun Xu[a], Wei Li[a], Zhongduo Xiong[b], Jinli Fang[a], Yuguang Li[a], Qiang Wang[a,b,*], Qingfu Zeng[b,*]

[a]*School of Chemistry and Chemical Engineering, Wuhan Textile University, Wuhan 430073, China, Tel. +86027 59367334; Fax: +86027 59367343; emails: xzjwtu@163.com (Z. Xu), liwei_wuse@qq.com (W. Li), 827898083@qq.com (J. Fang), liyg2010@wtu.edu.cn (Y. Li), qiang_wang@wtu.edu.cn (Q. Wang)*
[b]*Engineering Research Centre for Cleaner Production of Textile Printing and Dyeing, Ministry of Education, Wuhan 430073, China, emails: 121698686@qq.com (Z. Xiong), qfzeng@vip.sina.com (Q. Zeng)*

Received 15 October 2014; Accepted 21 January 2015

ABSTRACT

The amino-functionalized magnetic nanoadsorbent Fe_3O_4@SiO_2-NH_2 was prepared and it was characterized by X-ray powder diffraction, transmission electron microscopy, Fourier transform infrared (FT-IR) spectroscopy, and thermogravimetric analysis (TGA). The adsorption of anionic dyes including Acid Orange II (AO II) and Reactive Brilliant Red X-3B (X-3B) onto Fe_3O_4@SiO_2-NH_2 was investigated. The results showed that Fe_3O_4@SiO_2-NH_2 exhibited efficient adsorption for these anionic dyes under acidic conditions, and it was proposed to proceed via electrostatic attraction and hydrogen bonding between the positively charged protonated amino groups ($-NH_3^+$) on the adsorbent surface and the negatively charged sulfonate groups ($-SO_3^-$) of the dyes. The mechanism was supported by density functional theory (DFT) calculations. The adsorption kinetics for AO II and X-3B on Fe_3O_4@SiO_2-NH_2 followed the pseudo-second-order kinetic model, and the adsorption equilibrium data fitted well with Langmuir isotherm model. The maximum adsorption capacities for AO II and X-3B at pH 2 under room temperature were 132.2 and 233.1 mg g^{-1}, respectively. Desorption of dyes and regeneration of the adsorbent were carried out using aqueous solution at pH 10. The adsorbent Fe_3O_4@SiO_2-NH_2 could be easily recovered by external magnet and it exhibited good recyclability and reusability for three cycles use.

Keywords: Anionic dye removal; Adsorption; Wastewater treatment; Magnetic silica; Amino-functionalized nanoparticles

1. Introduction

Synthetic dyes are present in wastewater streams from many industrial sectors including textile, leather, cosmetics, paper, electronics, printing, plastic, pharmaceutical, food, etc. [1,2]. Many dyes and their degradation species are toxic and potentially carcinogenic to human beings, micro-organisms, and aquatic life [1,3–11]. Because of their complex molecular structures and large sizes, most of the dyes are stable against photodegradation, biodegradation, and oxidizing agents [7,8,12,13]. Various methods have been developed for the removal of dyes in

*Corresponding authors.

1944-3994/1944-3986 © 2015 Balaban Desalination Publications. All rights reserved.

wastewater. Since adsorption offers effectiveness, economy, flexibility, and simplicity in design, ease of operation with no unwanted side products, it is much better than other techniques like coagulation and flocculation, froth flotation, oxidation, biological process, and membrane separation [11,14–16]. Therefore, adsorption technique has found wide application in the removal of dyes, organic pollutants, and heavy metal ions from wastewater [3,8,9,17–23]. It is important to develop novel and cost-effective adsorption technologies for the treatment of wastewater. In the past few decades, various biosorbents including agricultural by-products and animal waste materials have been exploited for the removal of dyes from aqueous solution [8–11,18–22,24–27]. On the other hand, nanosized adsorbent has attracted increasing interest in recent years as it possesses good performance due to high specific surface area and the absence of internal diffusion resistance [16,28]. However, the small size of the particles makes their separation complex and the nanoadsorbents could not be separated easily from aqueous solution by filtration or centrifugation. This problem can be solved using magnetic nanoadsorbents as they can be manipulated by an external magnetic field [16,28,29]. Coating magnetic particles with modified silica and recovering them from solution by application of a magnetic field provide a cheap and effective method of particle separation [29,30]. Magnetic separation techniques have many applications in biochemistry, biology, analytical chemistry, mining ores, and wastewater treatment technology, etc. [13,29]. However, to the best of our knowledge, very little work has been found in the literature related to the use of amino-modified magnetic silica in removal of dyes from their aqueous solutions. In a previous paper, Donia and co-workers prepared magnetic silica through precipitation of silica in the presence of magnetite particles (Fe_3O_4) using sodium silicate solution and hydrochloric acid solution. The magnetic silica was then functionalized with amine groups. The adsorbent thus prepared showed a maximum adsorption capacity of 61.33 mg g^{-1} for dye acid orange 10 [31]. We have prepared silica-coated magnetic nanoparticles Fe_3O_4@SiO_2-NH_2 from a different approach via a sol–gel process according to a modified Stöber method [32,33], and the amino-functionalized adsorbent showed absorption capacities of 132.2 and 233.1 mg g^{-1} for Acid Orange II (AO II) and X-3B, respectively. Thus, the study of modified magnetic silica with higher dye removal efficiency still remains an interesting task that should not be underestimated. AO II and X-3B have been chosen as the model dyes in this study since they belong to the typical class of azo dyes, which are abundantly used in textile industries and are common industrial pollutants [6,16,17]. They have been reported to cause mutagenesis, chromosomal fractures, carcinogenesis, and respiratory toxicity [3,34–36].

We reported herein the preparation and characterization of amino-functionalized magnetic nanoadsorbent Fe_3O_4@SiO_2-NH_2. The dye absorption/desorption behavior and reusability of this adsorbent were investigated. The adsorption mechanism was further clarified based on experimental data and density functional theory (DFT) calculations. The kinetic and thermodynamic parameters of adsorption were also analyzed.

2. Experimental

2.1. Materials and methods

Tetraethyl orthosilicate (TEOS) and 3-aminopropyltrimethoxysilane (APTS) were obtained from Aladdin Reagent Co. Ltd, China. $FeCl_3{\cdot}6H_2O$, $FeSO_4{\cdot}7H_2O$, ammonium hydroxide (25%), sulfuric acid, sodium hydroxide, methanol, and ethanol were purchased from Sinopharm Chemical Reagents Co. Ltd, China. AO II and Reactive Brilliant Red X-3B (X-3B) were obtained from Sigma-Aldrich, and the chemical structures of the dyes are shown in Fig. 1. These chemicals and reagents were used as supplied without further purification. Dry toluene was distilled under N_2 from CaH_2, and dry methanol from magnesium methoxide. All aqueous solutions were prepared using double-distilled water, and the other reagents were of analytical grade (AR).

Fourier transform infrared (FT-IR) spectra were recorded using an AVATAR 360 spectrometer (Nicolet, USA), and KBr pellets were used for solid samples. Thermogravimetric analysis (TGA) of the samples was investigated using a Mettler Toledo TGA/DSC1 STARe System thermogravimetric analyzer. X-ray powder diffraction (XRD) patterns were recorded on an Empyrean diffractometer (PANalytical, B.V Company) with a Cu Kα radiation generated at

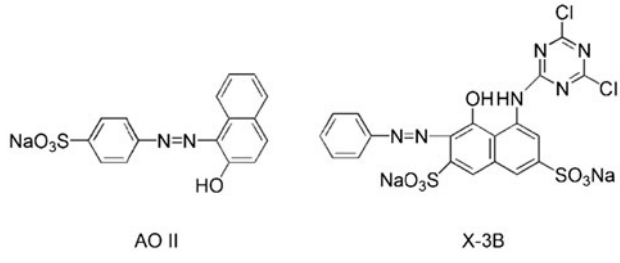

Fig. 1. Chemical structures of dyes AO II and X-3B.

40 kV and 40 mA. A JEM-2010 transmission electron microscope (TEM) (Japanese Electronic Optical Co. Ltd., Japan) was used to obtain the information about particle size and morphology of the samples. Concentration of the dye in the supernatant solution before and after adsorption was determined using a Varian Cary 50 Scan UV–vis spectrophotometer (Varian, USA). pH measurements were made using a Starter-3C digital pH meter (OHAUA Instrument (Shanghai) Co. Ltd, China). Ultrasound irradiation was carried out in an ultrasound clean bath (SB-5200D, Ningbo Scientz Biotechnology Co. Ltd., China) operating at a power of 200 W.

2.2. Synthesis

2.2.1. Preparation of magnetic nanoparticles (MNPs) Fe_3O_4

MNPs Fe_3O_4 were synthesized via modification of a literature method [37]. $FeCl_3{\cdot}6H_2O$ (2.70 g, 10 mmol) and $FeSO_4{\cdot}7H_2O$ (2.78 g, 10 mmol) were separately dissolved in distilled water, and the mixed Fe^{2+}/Fe^{3+} solution was added dropwise into 40 mL of an ammonia solution (3.5 mol L^{-1}) at 60°C under ultrasound irradiation. After reaction for 40 min, black Fe_3O_4 nanoparticles were collected by magnetic separation, washed with water to neutral pH, and then redispersed in ethanol for future use.

2.2.2. Preparation of magnetic silica (Fe_3O_4@SiO_2)

MNPs Fe_3O_4 were coated with a layer of SiO_2 film according to the following procedure [32,33]. MNPs Fe_3O_4 (0.9 g) were dispersed in a mixture of ethanol (60 mL) and ultrapure water (15 mL) by sonication for approximately 10 min. Ammonium hydroxide (10 mL, 25%) and TEOS (4 mL) were then consecutively added into the mixture. The mixture was stirred for 24 h at RT under a nitrogen gas atmosphere. The resulting light gray solid powder was collected by magnetic separation, washed with ultrapure water to neutral pH, and dried under vacuum.

2.2.3. Preparation of amino-functionalized magnetic silica (Fe_3O_4@SiO_2-NH_2)

In 20 mL of dry toluene, 0.3 g of Fe_3O_4@SiO_2 was suspended and 0.4 mL of 3-aminopropyltrimethoxysilane was added to the suspension. The reaction mixture was refluxed for 24 h under mechanical stirring and a nitrogen gas atmosphere. The brownish yellow solid was obtained by magnetic separation, washed with toluene and ethanol, respectively, and dried under vacuum.

2.3. Adsorption studies

Dye adsorption experiments were conducted at room temperature according to batch methods. The measurements were performed by mixing certain amount of adsorbent with dye solution in 100 mL flasks, and the mixture was shaken on an automatic shaker (IKA/KS 130 basic, IKA, Germany) at 560 rpm for a fixed period. At the end of the adsorption experiments, the adsorbents were separated by external magnet. Changes of the absorbance of AO II and X-3B solution samples were monitored and determined at certain time intervals by UV–vis spectroscopy at maximum wavelengths (λ_{max}) of 484 and 538 nm, respectively. Dye removal ratio (R%) was calculated according to the initial and equilibrium dye concentrations, respectively.

2.3.1. Effect of pH

The effect of pH on the adsorption of dyes on Fe_3O_4@SiO_2-NH_2 was investigated by placing 0.05 g of Fe_3O_4@SiO_2-NH_2 in a series of flasks containing 60 mL of AO II solution (200 mg L^{-1}) or X-3B solution (350 mg L^{-1}), respectively. Solutions containing 20 mg L^{-1} of AO II or 50 mg L^{-1} of X-3B, respectively, were used for the comparison experiments using 0.05 g of Fe_3O_4@SiO_2. The desired pH (from 2 to 8) was adjusted by diluted H_2SO_4 and NaOH solutions. The contents of the flasks were equilibrated on an automatic shaker at 560 rpm for 2 h.

2.3.2. Effect of adsorbent dosage

The effect of adsorbent dosage on dye adsorption on Fe_3O_4@SiO_2-NH_2 was investigated by contacting 60 mL of AO II solution (300 mg L^{-1}) or X-3B solution (400 mg L^{-1}) with different amounts of Fe_3O_4@SiO_2-NH_2 at pH 2. The contents of the flasks were equilibrated on an automatic shaker at 560 rpm for 2 h. Solutions containing 30 mg L^{-1} of AO II or 50 mg L^{-1} of X-3B, respectively, were used for the comparison experiments using Fe_3O_4@SiO_2.

2.3.3. Kinetic studies

The effect of contact time (from 0 to 120 min) on dye adsorption was studied by placing 0.02 g of Fe_3O_4@SiO_2-NH_2 in a series of flasks with each containing 30 mL of AO II solution (100 mg L^{-1}) or X-3B

solution (200 mg L^{-1}) at pH 2. The flasks were removed from the shaker at different time intervals and adsorbent was separated by external magnet. The residual concentrations of the dyes were then measured to calculate the amount of dyes adsorbed. Pseudo-first-order and pseudo-second-order models were applied, respectively, to analyze the adsorption kinetics.

2.3.4. Adsorption isotherms

The effect of the initial dye concentrations on dye removal was investigated by placing 0.03 g of Fe_3O_4@-SiO_2-NH_2 in a series of flasks containing 30 mL of dye solutions with the desired different initial concentrations (30–300 mg L^{-1} for AO II; 100–400 mg L^{-1} for X-3B) at pH 2. The flasks were shaken for 2 h at 560 rpm. The adsorbent was then separated by magnet, and the residual dye concentrations were determined to calculate the amount of dyes adsorbed. Langmuir and Freundlich models were used, respectively, to analyze the adsorption isotherms.

2.3.5. Desorption and reusability

With 60 mL of AO II solution (150 mg L^{-1}) or X-3B solution (300 mg L^{-1}), 0.1 g of Fe_3O_4@SiO_2-NH_2 was loaded, respectively, at pH 2 (the adsorption procedures described in Section 2.3.4 were used). The dye-loaded adsorbent was collected with external magnet and washed with distilled water to remove any unadsorbed dyes, and it was then shaken with 60 mL of a NaOH solution (pH 10) for 4 h to desorb dyes from the adsorbent. In order to test the reusability of Fe_3O_4@-SiO_2-NH_2, the adsorption–desorption cycles were repeated for three times to investigate the change of adsorption ratio and desorption ratio, respectively [28,30,31,38]. The ratio of desorption was calculated according to the amount of dyes desorbed to the stripping medium and the amount of dyes adsorbed onto the adsorbent.

2.4. Quantum chemical calculations

Geometry optimization of AO II and X-3B molecules and their interactions with the surface of Fe_3O_4@SiO_2-NH_2 were carried out using DFT calculations with ADF2013 program [39]. The ground-state geometry of AO II and X-3B with modeled molecules on the surface of Fe_3O_4@SiO_2-NH_2 was optimized by GGA-BLYP functional and TZVP basis set. An empirical van der Waals correction on DFT (DFT-D3) was adopted. For the D3 term, the damping of Johnson and Becke was employed [40].

3. Results and discussion

3.1. Synthesis and characterization

The preparation of magnetic adsorbent Fe_3O_4@-SiO_2-NH_2 and its precursors MNPs Fe_3O_4 and Fe_3O_4@-SiO_2 is described in Fig. 2. MNPs Fe_3O_4 were synthesized via modification of a literature method of reverse co-precipitation using $FeCl_3$ and $FeSO_4$ as iron sources under ultrasonic irradiation [37]. A layer of SiO_2 was coated onto Fe_3O_4 nanoparticles using a modified Stöber method, resulting in the formation of silica coated core-shell nanoparticles Fe_3O_4@SiO_2 [32,33,41]. The grafting of APTS onto Fe_3O_4@SiO_2 to form Fe_3O_4@SiO_2-NH_2 was achieved by coupling reaction between silanol groups of silica on Fe_3O_4@SiO_2 and methoxy groups of APTS to yield the new surface with functional groups of amine.

TEM was applied to reveal the dimension and surface morphology of nanoparticles. The nanoparticles of Fe_3O_4 are generally homogeneous and spherical with the diameters mainly ranging from 15 to 20 nm. The introduction of silica coating to the surface of magnetic nanoparticles was concluded from TEM images. The particle size was vividly increased after coating with silica, due to the agglomeration of Fe_3O_4 inside nanospheres and surface growth of silica on the shell [42]. Fe_3O_4@SiO_2 nanoparticles presented roughly spherical core-shell structure and the gray outer layer around the magnetic Fe_3O_4 nanoparticle was amorphous silica coating [43]. Amino-functionalized particles showed an aggregation which could be assigned to the self-interaction of the surrounding layer of amines [16,44]. No significant change was found in the spherical shape and particle size, suggesting that amino modification had no effect on the inner core materials [41].

XRD patterns of Fe_3O_4, Fe_3O_4@SiO_2, and Fe_3O_4@-SiO_2-NH_2 were investigated. Six characteristic peaks for Fe_3O_4 were observed at $2\theta = 30.2^o$, 35.5^o, 43.3^o, 53.6^o, $57.2^{o,}$ and 62.7^o [32,37,41]. The XRD patterns of Fe_3O_4@SiO_2 and Fe_3O_4@SiO_2-NH_2 showed good identity with that of the Fe_3O_4 structure, suggesting that the magnetic Fe_3O_4 nanospheres were successfully encapsulated by the amorphous silica layer and further amino-functionalization did not affect the original crystallinity of Fe_3O_4 structure [16,32,41,45].

FT-IR analysis was performed to elucidate the active sites present on the surface of Fe_3O_4, Fe_3O_4@-SiO_2, and Fe_3O_4@SiO_2-NH_2. The peak at 580 cm^{-1} is the typical absorption of Fe–O vibration in Fe_3O_4. The spectrum of Fe_3O_4@SiO_2 exhibits the characteristic peaks at 1,100, 800, and 470 cm^{-1}, corresponding to the typical symmetric and bending vibrations of Si–O–Si, respectively, in the supporting framework of

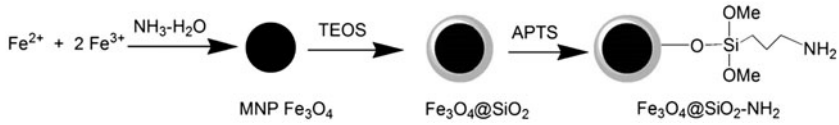

Fig. 2. Preparation of MNPs Fe_3O_4, Fe_3O_4@SiO_2, and Fe_3O_4@SiO_2-NH_2.

silica [30,31,33,41]. The absorption peaks of 3,450 and 1,650 cm^{-1} are observed in all the spectra corresponding to the stretching vibration and bending vibration of O–H group of water, respectively. The spectrum of amino-modified magnetic silica Fe_3O_4@SiO_2-NH_2 displays mainly the same characteristic bands of Fe_3O_4@-SiO_2 with decreased absorption intensity of the free silanol group at 980 cm^{-1} [6,46]. New bands at about 2,900 cm^{-1} in the spectra of Fe_3O_4@SiO_2-NH_2 are the characteristic absorption of aliphatic C–H stretching vibrations. The new peak around 1,570 cm^{-1} in the spectra of Fe_3O_4@SiO_2-NH_2 is attributed to the absorption of NH_2 group [47]. FT-IR spectra not only confirmed the silica coating onto the surface of magnetic Fe_3O_4 particles but also verified the surface modification of Fe_3O_4@SiO_2 to yield Fe_3O_4@SiO_2-NH_2 [41].

To have an insight into the thermal degradation behaviors of the prepared adsorbents, TGA analysis was carried out and the results are shown in Fig. 3. The weight loss in the 50–200°C interval is assigned to physisorbed water molecules released from samples, while the weight loss above 500°C for Fe_3O_4 and Fe_3O_4@SiO_2 is associated with the release of hydroxyl ions from the particles or condensation of silanol groups bonded to the silica surface [30,47]. As expected, the functional surfaces of Fe_3O_4@SiO_2-NH_2 presented different stages of mass loss. The first mass losses in the 50–250°C range are assigned to adsorbed water and the second losses at 250–600°C are attributed to the organic groups immobilized on silica surfaces. The mass losses at 600–1,000°C are related to the decomposition of aminopropyl groups immobilized on the surfaces and the condensation of the remaining silanols to yield siloxane groups, resulting in water loss and breaking of organic groups. The increase in mass losses of Fe_3O_4@SiO_2-NH_2 relative to Fe_3O_4@SiO_2 is in agreement with the aminopropyl chains covalently attached to the surface of Fe_3O_4@-SiO_2-NH_2. This observation is in well agreement with FT-IR results, clearly illustrating the introduction of amino moieties onto Fe_3O_4@SiO_2-NH_2. It is also of note that the total weight loss of dye-loaded Fe_3O_4@-SiO_2-NH_2 is obviously higher than that of pristine Fe_3O_4@SiO_2-NH_2, and this is caused by extra organic components of dyes loaded onto Fe_3O_4@SiO_2-NH_2. The weight loss of dye-loaded Fe_3O_4@SiO_2 is similar to that of untreated Fe_3O_4@SiO_2, suggesting that the dye adsorption ability of Fe_3O_4@SiO_2 was very small (also see experimental adsorption results in the following parts).

3.2. Adsorption studies

3.2.1. Effect of pH on dye adsorption

pH of the aqueous solution is an important operational parameter in the adsorption process, since pH values affect not only protonation of the functional

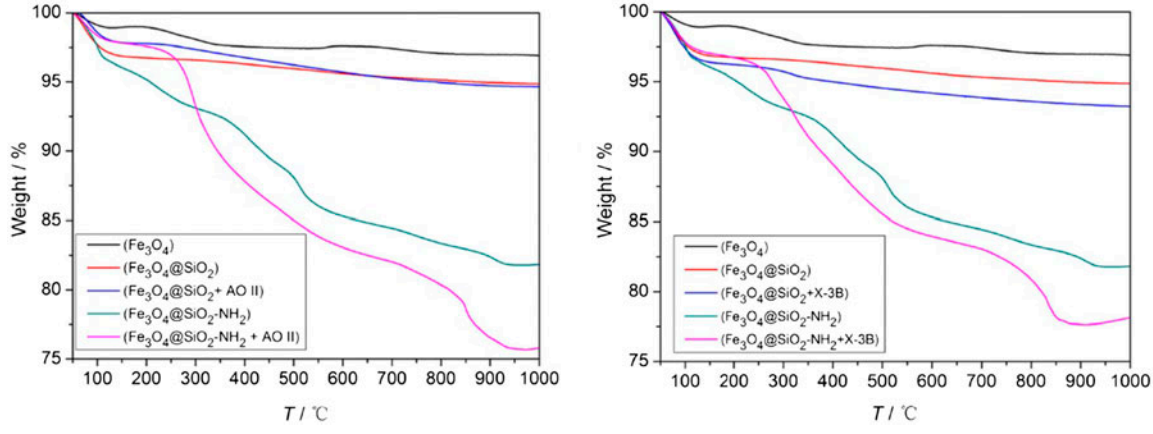

Fig. 3. TGA curves of Fe_3O_4@SiO_2-NH_2 and its precursors before and after dye adsorption.

groups of the adsorbent, but also the speciation of dye molecules in solution [30,45]. The effect of pH on the adsorption of AO-II and X-3B on Fe_3O_4@SiO_2-NH_2 is shown in Fig. 4. The adsorption capacity increased when the pH was decreased and the maximum adsorption was observed at pH 2. The efficient adsorption of AO-II and X-3B at acidic conditions may be due to electrostatic attraction and hydrogen bonding between the positively charged protonated amino groups on the silica surface ($-NH_3^+$) and the negatively charged sulfonate groups ($-SO_3^-$) of the dyes. The preliminary mechanism is described as following [1,2,6,31,46]:

$$Fe_3O_4@SiO_2 - NH_2 + H_2SO_4 \rightarrow Fe_3O_4@SiO_2 - NH_3^+ \cdots HSO_4^-$$

$$Fe_3O_4@SiO_2 - NH_3^+ \cdots HSO_4^- + D - SO_3^-Na^+ \rightarrow Fe_3O_4@SiO_2 - NH_3^+ \cdots {}^-O_3S - D + NaHSO_4$$

It may be proposed that a significantly high electrostatic attraction existed at pH 2. The adsorption decreased as the pH of the medium increased, and this may be attributed to the deprotonation of amino groups along with the formation of negatively charged silanolate groups ($\equiv SiO^-$) that repel the sulfonate groups ($-SO_3^-$) of the dye from interaction with the surface [6,31]. The experiments were not conducted at pH smaller than 2, as the anchored aminopropyl moiety on the silica surface may be removed in such conditions [2,48]. The effective pH of 2 was used in further studies. The results in Fig. 4 also indicate that magnetic silica Fe_3O_4@SiO_2 without surface amino-functionalization showed very low ability for dye removal. These results clearly confirm that the amino groups worked as efficient sites for dye adsorption under the performed conditions.

The geometry-optimized DFT models of the interaction between the modeled surface of Fe_3O_4@SiO_2-NH_2 and the dyes are shown in Fig. 5. DFT calculated models indicate that AO-II or X-3B interacts with the adsorbent surface through electrostatic attraction as well as hydrogen bond formation through the negatively charged sulfonate groups ($-SO_3^-$) and positively charged ammonium groups ($-NH_3^+$) [2,6,31].

3.2.2. Effect of adsorbent dosage

The effect of adsorbent dosage on dye removal is shown in Fig. 6. The increase of dye adsorption along with increased adsorbent dosage may be due to the increased adsorbent surface and availability of more adsorption sites [7,46]. The results in Fig. 6 also show that dye removal ability of Fe_3O_4@SiO_2-NH_2 is much higher than that of Fe_3O_4@SiO_2, confirming that the amino groups worked as efficient sites for dye adsorption under the performed conditions.

3.2.3. Kinetic studies

Fast adsorption is important for wastewater treatment. The removal of dyes by Fe_3O_4@SiO_2-NH_2 was rapid in the initial stages of adsorption and gradually decreased with time until equilibrium reached at about 45 min. The rapid adsorption observed during the initial stages may be due to the abundant availability of active sites on the adsorbent surface, whereas the adsorption becomes less efficient with the gradual occupancy of these sites. The fast adsorption rate may mainly be attributed to the electrostatic interactions [14].

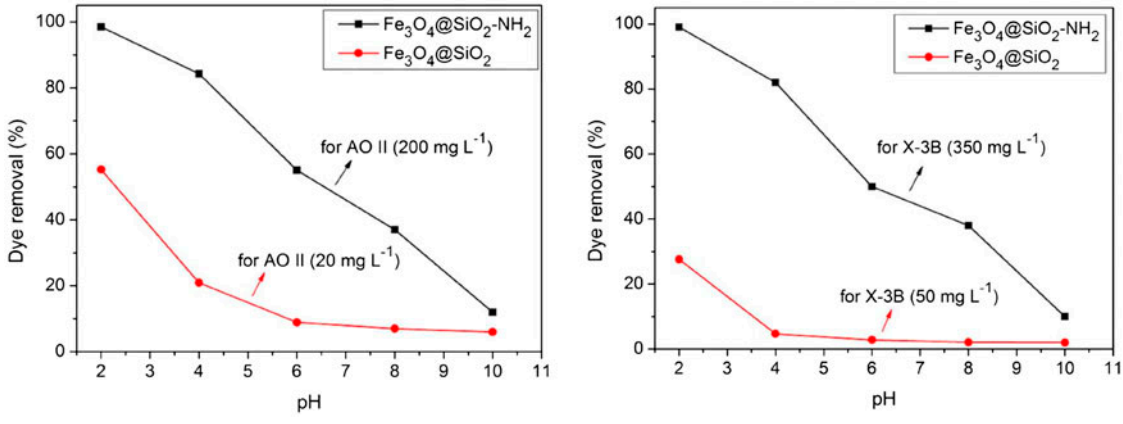

Fig. 4. Effect of pH on dye removal by Fe_3O_4@SiO_2-NH_2 and Fe_3O_4@SiO_2.

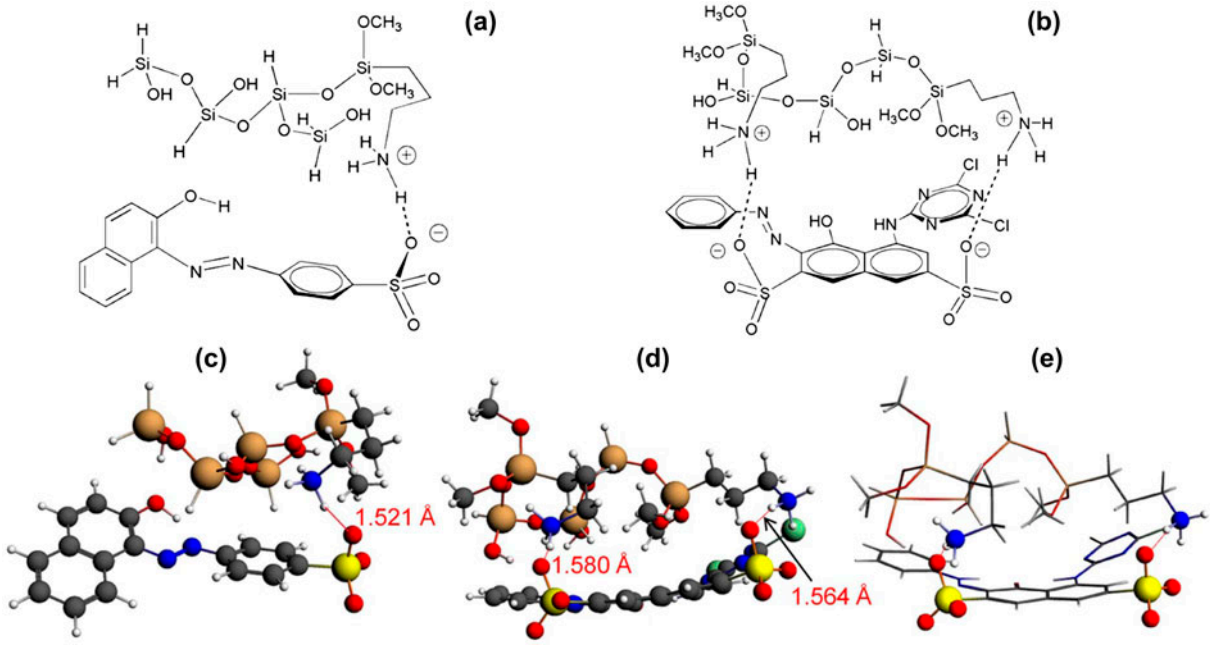

Fig. 5. Proposed mechanism of interactions between dyes and the modeled surface of Fe_3O_4@SiO_2-NH_2 (with numbers showing the distance between the (N)H···O(S) part of hydrogen bond). (a) and (b) chemical structure diagrams showing the interaction for AO II or X-3B, respectively; (c) DFT model showing the interaction for AO II; (d) DFT model showing the interaction for X-3B; (e) wireframe drawing of (d) for clarity.

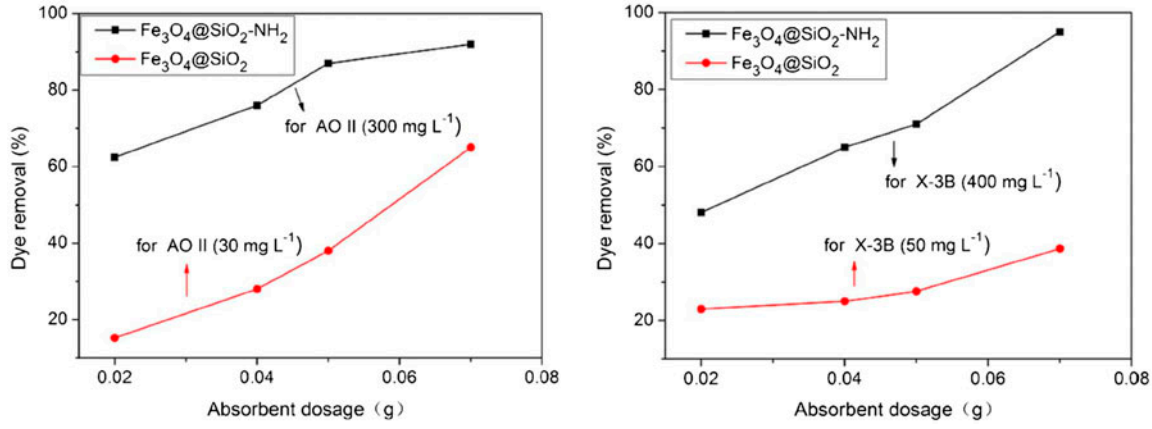

Fig. 6. Effect of adsorbent dosage on the adsorption of dyes on Fe_3O_4@SiO_2-NH_2 or Fe_3O_4@SiO_2.

In order to investigate the mechanism of adsorption and the main parameters governing adsorption kinetics, empirically obtained kinetic adsorption data were fitted to the pseudo-first-order and pseudo-second-order models shown in Eqs. (1) and (2), respectively. Each of these models has been widely used to describe metal and organic adsorption on adsorbents [46,49,50].

$$\ln(q_e - q_t) = \ln q_e - k_1 t \quad (1)$$

$$\frac{t}{q_t} = \frac{1}{k_2 q_e^2} + \frac{t}{q_e} \quad (2)$$

where q_e and q_t (mg g^{-1}) are the adsorption capacities at equilibrium and at time t, respectively; k_1 (min^{-1}) and k_2 (g mg^{-1} min^{-1}) are the rate constants of the pseudo-first-order adsorption and the pseudo-second-order adsorption, respectively. The calculated kinetics parameters and the correlation coefficients (R^2) are given in Table 1.

Table 1
Kinetic model parameters for the adsorption of AO II and X-3B on Fe_3O_4@SiO_2-NH_2

Dyes	$q_{e\ (Exp.)}$ (mg g^{-1})	Pseudo-first-order model			Pseudo-second-order model		
		k_1 (min^{-1})	$q_{e\ (Cal.)}$ (mg g^{-1})	R^2	k_2 (g mg^{-1} min^{-1})	$q_{e\ (Cal.)}$ (mg g^{-1})	R^2
AO II	101.01	0.03479	28.98	0.8199	0.004825	99.50	0.9950
X-3B	240.38	0.03315	128.09	0.9634	0.000999	240.96	0.9910

The pseudo-second-order model equation provides an excellent fit between the predicted curves and the experimental values, whereas the pseudo-first-order kinetics does not fit well to the experimental data. The correlation coefficients (R^2) of the pseudo-second-order kinetic model ($R^2 > 0.99$) are much higher than that of the pseudo-first-order model. In addition, the experimental values of $q_{e\ (Exp.)}$ are very similar to the values calculated by the pseudo-second-order equation ($q_{e\ (Cal.)}$). Thus, the adsorption can be better described by the pseudo-second-order kinetic model rather than the pseudo-first-order kinetic model [38]. The best fit of the second-order expression suggests that the chemisorption mechanism is involved in the adsorption [51,52].

3.2.4. Adsorption isotherm

The adsorption isotherms of AO II and X-3B, respectively, are shown in Fig. 7. Adsorption isotherms of AO II and X-3B are of very similar pattern and they indicate that the equilibrium adsorption amount increases rapidly with the increase of equilibrium concentrations of dye species. This implies that Fe_3O_4@SiO_2-NH_2 possesses very strong adsorption ability and high affinity for AO II and X-3B [53,54]. In order to evaluate the adsorption characteristics of AO II and X-3B on Fe_3O_4@SiO_2-NH_2, experimental data were fitted to the two well-known adsorption isotherm models of Langmuir and Freundlich as represented in Eqs. (3) and (4), respectively [1,6,31,46].

$$\frac{C_e}{q_e} = \frac{C_e}{q} + \frac{1}{qk_L} \tag{3}$$

$$\ln q_e = \ln k_F + \frac{\ln C_e}{n} \tag{4}$$

where q_e is the amount of dye adsorbed on the adsorbent (mg g^{-1}), C_e is the equilibrium dye concentration in the solution (mg L^{-1}), q is the maximum adsorption capacity at monolayer coverage, k_L is the Langmuir adsorption constant (L mg^{-1}), k_F is the binding energy constant reflecting affinity of adsorbents to dye species, and n is the Freundlich exponent related to adsorption intensity.

Table 2 lists the parameters of the Langmuir and Freundlich models along with the regression coefficients (R^2). The R^2 values in Table 2 reveal that the Langmuir isotherm fits the experimental results better than Freundlich model, implying that the adsorption of AO II and X-3B onto Fe_3O_4@SiO_2-NH_2 follows the mechanism of monolayer adsorption (chemisorption) on a homogenous surface [1,4–6,31,38,46,55]. Table 2 shows that the maximum adsorption capacity of

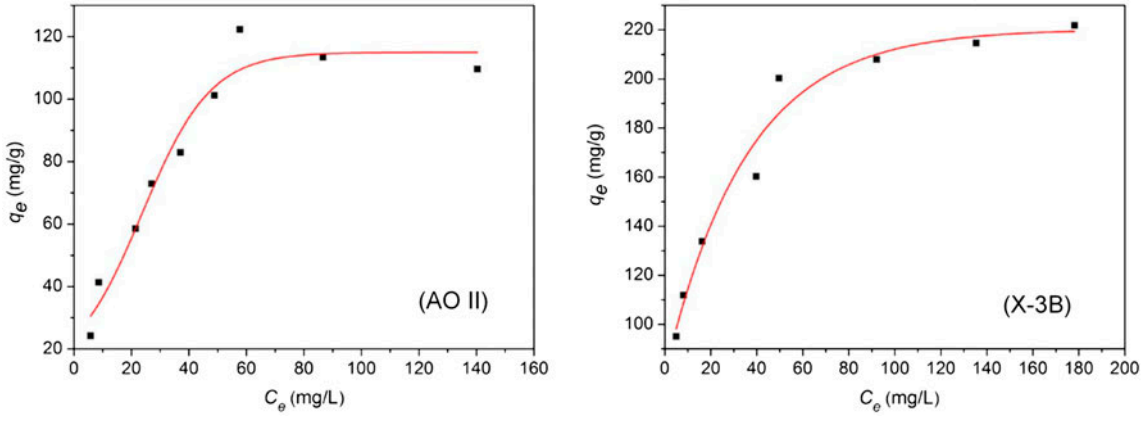

Fig. 7. Adsorption isotherms for AO II and X-3B on Fe_3O_4@SiO_2-NH_2.

Table 2
The isotherm parameters for the adsorption of AO II and X-3B on Fe_3O_4@SiO_2-NH_2

	Langmuir model			Freundlich model		
Dyes	q (mg g^{-1})	k_L (L mg^{-1})	R^2	k_F (mg g^{-1})	n	R^2
AO II	132.2	0.0051	0.9754	13.07	2.027	0.8967
X-3B	233.1	0.093	0.9967	67.427	4.118	0.9543

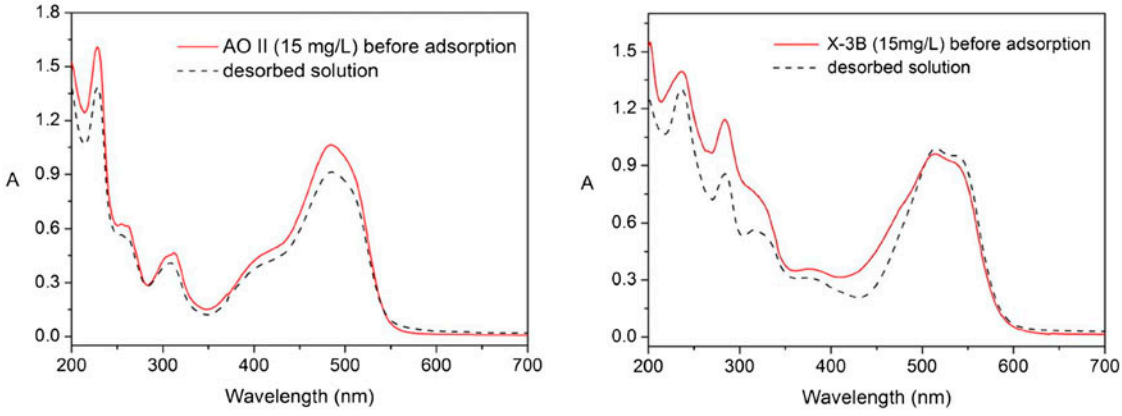

Fig. 8. UV–vis spectra for the solutions containing pristine dyes or the desorbed dyes.

Fe_3O_4@SiO_2-NH_2 for AO II and X-3B is 132 and 233 mg g^{-1}, respectively. These values are comparable or higher than that of other synthetic or natural inorganic and agricultural by-products adsorbents reported in literature for the adsorption of dyes with similar structure to AO II and X-3B, respectively. These adsorbents include, for example, functionalized amorphous and mesoporous silica gel [6,15], activated carbon, multi-walled carbon nanotubes, anion exchange membrane [13], amine-functionalized silica nanoparticles [46], zeolites, clay [4,15], agricultural products, chitosan [3,15], and nanoporous silica SBA-3 [6,15,38,56]. It is of note that the adsorption capacity of Fe_3O_4@SiO_2-NH_2 for X-3B is similar to that of nanoporous silica SBA-3 (294 mg g^{-1}) [56], while ammonium-functionalized MCM-41 displayed an adsorption capacity of 209 mg g^{-1} for X-3B. Fe_3O_4 MNPs coated by aminoguanidine showed an adsorption capacity of 119 mg g^{-1} for AO 20, which is a structural isomer of AO II [38], whereas amine-modified silica only had an adsorption capacity of 14.3 mg g^{-1} for AO 12 at RT [6].

3.3. Desorption and reusability

The regeneration and reuses of the adsorbent are important for potential practical applications [57]. From the study of pH effect, it was found that the adsorption of AO II and X-3B on Fe_3O_4@SiO_2-NH_2 decreased when the solution pH was increased. This result suggested that desorption of dyes and regeneration of the adsorbent were possible by adjusting the pH of the regenerating media.

Desorption of the adsorbed dyes was carried out with diluted NaOH solution at pH 10. The solution containing desorbed dyes showed essentially the same UV–vis spectra as the untreated dye solution (Fig. 8), and this was attributed to the deprotonation of the amine groups under basic conditions [31]. It also confirmed that the electrostatic interaction was involved in the adsorption of anionic dyes onto the adsorbent Fe_3O_4@SiO_2-NH_2 [38].

The recyclable use of adsorbent and dyes (desorption) can be accomplished using external magnet and adjusting pH of the media. The regeneration and reusability of the adsorbent was evaluated after the first desorption/regeneration process. The reusability was checked by following the adsorption–desorption processes as described in Section 2.3.5 for three cycles and the adsorption/desorption efficiency in each cycle was determined. The results showed that the adsorption and desorption efficiency of Fe_3O_4@SiO_2-NH_2 for both AO II and X-3B in the third cycle still retained a ratio of 89–91%, indicating that Fe_3O_4@SiO_2-NH_2 possesses a good reusability and may be used for further dye adsorption [28].

4. Conclusion

Magnetic nanoadsorbent $Fe_3O_4@SiO_2$-NH_2 was prepared by surface modification of $Fe_3O_4@SiO_2$ with APTS to immobilize the amino-functionalized groups. The maximum adsorption capacities of $Fe_3O_4@SiO_2$-NH_2 for AO II and X-3B at pH 2 were 132.2 and 233.1 mg g^{-1}, respectively. Experimental results and DFT calculations confirmed that the mechanism of high adsorption capacity for anionic dyes in acidic solution was attributed to the electrostatic attraction and hydrogen bonding between the positively charged protonated amino groups on the adsorbent surface ($-NH_3^+$) and the negatively charged sulfonate groups ($-SO_3^-$) of the dyes. The kinetics for the adsorption of AO II and X-3B on $Fe_3O_4@SiO_2$-NH_2 followed the pseudo-second-order kinetic model, and the adsorption of AO II and X-3B on $Fe_3O_4@SiO_2$-NH_2 fitted well with Langmuir isotherm model. The good reusability and convenient magnetic separability make $Fe_3O_4@SiO_2$-NH_2 an efficient and recyclable adsorbent for removal of anionic dyes from polluted water. Current work is continuing in our laboratory to investigate the applications of adsorbent $Fe_3O_4@SiO_2$-NH_2 and its analogs for more complex dye solutions.

Acknowledgments

This work was financially supported by the National Natural Science Foundation of China (grant number 21277106 and 21101122); Scientific Research Foundation for Returned Overseas Chinese Scholars, State Education Ministry; Natural Science Foundation of Hubei Province (2008CDB038); Scientific Research Program of the Educational Department of Hubei Province (D20091703).

References

[1] M. Anbia, S. Salehi, Removal of acid dyes from aqueous media by adsorption onto amino-functionalized nanoporous silica SBA-3, Dyes Pigm. 94 (2012) 1–9.
[2] F. Rehman, P.L.O. Volpe, C. Airoldi, Free amino and imino-bridged centres attached to organic chains bonded to structurally ordered silica for dye removal from aqueous solution, J. Environ. Manage. 133 (2014) 135–143.
[3] M.T. Yagub, T.K. Sen, S. Afroze, H.M. Ang, Dye and its removal from aqueous solution by adsorption: A review, Adv. Colloid Interface 209 (2014) 172–184.
[4] E. Errais, J. Duplay, F. Darragi, I. M'Rabet, A. Aubert, F. Huber, G. Morvan, Efficient anionic dye adsorption on natural untreated clay: Kinetic study and thermodynamic parameters, Desalination 275 (2011) 74–81.
[5] M.A.M. Salleh, D.K. Mahmoud, W.A.W.A. Karim, A. Idris, Cationic and anionic dye adsorption by agricultural solid wastes: A comprehensive review, Desalination 280 (2011) 1–13.
[6] A.M. Donia, A.A. Atia, W.A. Al-amrani, A.M. El-Nahas, Effect of structural properties of acid dyes on their adsorption behaviour from aqueous solutions by amine modified silica, J. Hazard. Mater. 161 (2009) 1544–1550.
[7] N.F. Cardoso, R.B. Pinto, E.C. Lima, T. Calvete, C.V. Amavisca, B. Royer, M.L. Cunha, T.H.M. Fernandes, I.S. Pinto, Removal of remazol Black B textile dye from aqueous solution by adsorption, Desalination 269 (2011) 92–103.
[8] A. Mittal, V. Thakur, J. Mittal, H. Vardhan, Process development for the removal of hazardous anionic azo dye Congo red from wastewater by using hen feather as potential adsorbent, Desalin. Water Treat. 52 (2014) 227–237.
[9] J. Mittal, V. Thakur, A. Mittal, Batch removal of hazardous azo dye Bismark Brown R using waste material hen feather, Ecol. Eng. 60 (2013) 249–253.
[10] S. Nausheen, H.N. Bhatti, Z. Furrukh, S. Sadaf, S. Noreen, Adsorptive removal of Drimarine Red HF-3D dye from aqueous solution using low-cost agricultural waste: Batch and column study, Chem. Ecol. 30 (2014) 376–392.
[11] S. Sadaf, H.N. Bhatti, S. Nausheen, S. Noreen, Potential use of low-cost lignocellulosic waste for the removal of Direct Violet 51 from aqueous solution: Equilibrium and breakthrough studies, Arch. Environ. Contam. Toxicol. 66 (2014) 557–571.
[12] B. Kayan, B. Gözmen, M. Demirel, A.M. Gizir, Degradation of Acid Red 97 dye in aqueous medium using wet oxidation and electro-Fenton techniques, J. Hazard. Mater. 177 (2010) 95–102.
[13] W. Konicki, I. Pełech, E. Mijowska, I. Jasińska, Adsorption kinetics of acid dye Acid Red 88 onto magnetic multi-walled carbon nanotubes-Fe_3C nanocomposite, CLEAN—Soil, Air, Water 42 (2014) 284–294.
[14] J. Liu, S. Ma, L. Zang, Preparation and characterization of ammonium-functionalized silica nanoparticle as a new adsorbent to remove methyl orange from aqueous solution, Appl. Surf. Sci. 265 (2013) 393–398.
[15] L.S. Silva, L.C.B. Luciano, C.B. Lima, F.C. Silva, J.M.E. Matos, M.R.M.C. Santos, L.S.S. Júnior, K.S. Sousa, E.C.d.S. Filho, Dye anionic sorption in aqueous solution onto a cellulose surface chemically modified with aminoethanethiol, Chem. Eng. J. 218 (2013) 89–98.
[16] T. Poursaberi, M. Hassanisadi, Magnetic removal of Reactive Black 5 from wastewater using ionic liquid grafted-magnetic nanoparticles, CLEAN—Soil, Air, Water 41 (2013) 1208–1215.
[17] T.K. Saha, N.C. Bhoumik, S. Karmaker, M.G. Ahmed, H. Ichikawa, Y. Fukumori, Adsorption characteristics of Reactive Black 5 from aqueous solution onto chitosan, CLEAN—Soil, Air, Water 39 (2011) 984–993.
[18] H. Daraei, A. Mittal, M. Noorisepehr, F. Daraei, Kinetic and equilibrium studies of adsorptive removal of phenol onto eggshell waste, Environ. Sci. Pollut. Res. 20 (2013) 4603–4611.
[19] H. Daraei, A. Mittal, J. Mittal, H. Kamali, Optimization of Cr(VI) removal onto biosorbent eggshell membrane: Experimental & theoretical approaches, Desalin. Water Treat. 52 (2014) 1307–1315.

[20] J. Mittal, D. Jhare, H. Vardhan, A. Mittal, Utilization of bottom ash as a low-cost sorbent for the removal and recovery of a toxic halogen containing dye Eosin Yellow, Desalin. Water Treat. 52 (2014) 4508–4519.
[21] H. Daraei, A. Mittal, M. Noorisepehr, J. Mittal, Separation of chromium from water samples using eggshell powder as a low-cost sorbent: Kinetic and thermodynamic studies, Desalin. Water Treat. 53 (2015) 214–220.
[22] G. Sharma, M. Naushad, D. Pathania, A. Mittal, G.E. Eldesoky, Modification of *Hibiscus cannabinus* fiber by graft copolymerization: Application for dye removal, Desalin. Water Treat. doi: 10.1080/19443994.2014.904822.
[23] M. Naushad, A. Mittal, M. Rathore, V. Gupta, Ion-exchange kinetic studies for Cd(II), Co(II), Cu(II), and Pb (II) metal ions over a composite cation exchanger, Desalin. Water Treat. doi: 10.1080/19443994.2014.904823.
[24] S. Sadaf, H.N. Bhatti, Evaluation of peanut husk as a novel, low cost biosorbent for the removal of Indosol Orange RSN dye from aqueous solutions: Batch and fixed bed studies, Clean Technol. Environ. Policy 16 (2014) 527–544.
[25] S. Nawaz, H.B. Bhatti, T.H. Bokhari, S. Sadaf, Removal of Novacron Golden Yellow dye from aqueous solutions by low-cost agricultural waste: Batch and fixed bed study, Chem. Ecol. 30 (2014) 52–65.
[26] S. Sadaf, H.N. Bhatti, Batch and fixed bed column studies for the removal of Indosol Yellow BG dye by peanut husk, J. Taiwan Inst. Chem. Eng. 45 (2014) 541–553.
[27] S. Sadaf, H.N. Bhatti, S. Ali, K. Rehman, Removal of Indosol Turquoise FBL dye from aqueous solution by bagasse, a low cost agricultural waste: Batch and column study, Desalin. Water Treat. 52 (2014) 184–198.
[28] L. Zhou, J. Jin, Z. Liu, X. Liang, C. Shang, Adsorption of acid dyes from aqueous solutions by the ethylenediamine-modified magnetic chitosan nanoparticles, J. Hazard. Mater. 185 (2011) 1045–1052.
[29] S. Linley, T. Leshuk, F.X. Gu, Magnetically separable water treatment technologies and their role in future advanced water treatment: A patent review, CLEAN—Soil, Air, Water 41 (2013) 1152–1156.
[30] Q. Wang, W. Gao, Y. Liu, J. Yuan, Z. Xu, Q. Zeng, Y. Li, M. Schröder, Simultaneous adsorption of Cu(II) and SO_4^{2-} ions by a novel silica gel functionalized with a ditopic zwitterionic Schiff base ligand, Chem. Eng. J. 250 (2014) 55–65.
[31] A.A. Atia, A.M. Donia, W.A. Al-Amrani, Adsorption/desorption behavior of Acid Orange 10 on magnetic silica modified with amine groups, Chem. Eng. J. 150 (2009) 55–62.
[32] T. Jing, H. Du, Q. Dai, H. Xia, J. Niu, Q. Hao, S. Mei, Y. Zhou, Magnetic molecularly imprinted nanoparticles for recognition of lysozyme, Biosens. Bioelectron. 26 (2010) 301–306.
[33] Q. Chang, L. Zhu, C. Yu, H. Tang, Synthesis and properties of magnetic and luminescent Fe_3O_4/SiO_2/Dye/SiO_2 nanoparticles, J. Lumin. 128 (2008) 1890–1895.
[34] M. Kousha, E. Daneshvar, M.S. Sohrabi, M. Jokar, A. Bhatnagar, Adsorption of Acid Orange II dye by raw and chemically modified brown macroalga *Stoechospermum marginatum*, Chem. Eng. J. 192 (2012) 67–76.
[35] G.R. Xu, Y.P. Zhang, G.B. Li, Degradation of azo dye Active Brilliant Red X-3B by composite ferrate solution, J. Hazard. Mater. 161 (2009) 1299–1305.
[36] L. Tan, Y. Qu, J. Zhou, F. Ma, A. Li, Dynamics of microbial community for X-3B wastewater decolorization coping with high-salt and metal ions conditions, Bioresour. Technol. 100 (2009) 3003–3009.
[37] N. Wang, L. Zhu, D. Wang, M. Wang, Z. Lin, H. Tang, Sono-assisted preparation of highly-efficient peroxidase-like Fe_3O_4 magnetic nanoparticles for catalytic removal of organic pollutants with H_2O_2, Ultrason. Sonochem. 17 (2010) 526–533.
[38] D.P. Li, Y.R. Zhang, X.X. Zhao, B.X. Zhao, Magnetic nanoparticles coated by aminoguanidine for selective adsorption of acid dyes from aqueous solution, Chem. Eng. J. 232 (2013) 425–433.
[39] ADF, SCM, Theoretical Chemistry, Vrije Universiteit, Amsterdam, 2013. Available from: http://www.scm.com.
[40] S. Grimme, S. Ehrlich, L. Goerigk, Effect of the damping function in dispersion corrected density functional theory, J. Comput. Chem. 32 (2011) 1456–1465.
[41] S. Lan, X. Wu, L. Li, M. Li, F. Guo, S. Gan, Synthesis and characterization of hyaluronic acid-supported magnetic microspheres for copper ions removal, Colloids Surf., A 425 (2013) 42–50.
[42] M. Esmaeilpour, A.R. Sardarian, J. Javidi, Schiff base complex of metal ions supported on superparamagnetic Fe_3O_4@SiO_2 nanoparticles: An efficient, selective and recyclable catalyst for synthesis of 1,1-diacetates from aldehydes under solvent-free conditions, Appl. Catal., A 445–446 (2012) 359–367.
[43] S. Xuan, F. Wang, X. Gong, S.K. Kong, J.C. Yu, K.C.F. Leung, Hierarchical core/shell Fe_3O_4@SiO_2@γ-AlOOH@Au micro/nanoflowers for protein immobilization, Chem. Commun. 47 (2011) 2514–2516.
[44] Y. Jiang, C. Guo, H. Xia, I. Mahmood, C. Liu, H. Liu, Magnetic nanoparticles supported ionic liquids for lipase immobilization: Enzyme activity in catalyzing esterification, J. Mol. Catal. B: Enzym. 58 (2009) 103–109.
[45] Y. Ren, H.A. Abbood, F. He, H. Peng, K. Huang, Magnetic EDTA-modified chitosan/SiO_2/Fe_3O_4 adsorbent: Preparation, characterization, and application in heavy metal adsorption, Chem. Eng. J. 226 (2013) 300–311.
[46] N.M. Mahmoodi, S. Khorramfar, F. Najafi, Amine-functionalized silica nanoparticle: Preparation, characterization and anionic dye removal ability, Desalination 279 (2011) 61–68.
[47] J. Zhang, S. Zhai, S. Li, Z. Xiao, Y. Song, Q. An, G. Tian, Pb(II) removal of Fe_3O_4@SiO_2-NH_2 core-shell nanomaterials prepared via a controllable sol-gel process, Chem. Eng. J. 215–216 (2013) 461–471.
[48] A.R. Cestari, E.F.S. Vieira, G.S. Vieira, L.E. Almeida, Aggregation and adsorption of reactive dyes in the presence of an anionic surfactant on mesoporous aminopropyl silica, J. Colloid Interface Sci. 309 (2007) 402–411.
[49] M. Arshadi, F.S. Vahid, J.W.L. Salvacion, M. Soleymanzadeh, A practical organometallic decorated nano-size SiO_2–Al_2O_3 mixed-oxides for Methyl Orange removal from aqueous solution, Appl. Surf. Sci. 280 (2013) 726–736.
[50] S.A. Ahmed, E.M. Soliman, Silica coated magnetic particles using microwave synthesis for removal of dyes from natural water samples: Synthesis, characterization, equilibrium, isotherm and kinetics studies, Appl. Surf. Sci. 284 (2013) 23–32.

[51] E. Rosales, M. Pazos, M.A. Sanromán, T. Tavares, Application of zeolite-Arthrobacter viscosus system for the removal of heavy metal and dye: Chromium and Azure B, Desalination 284 (2012) 150–156.
[52] S. Wang, J. Wei, S. Lv, Z. Guo, F. Jiang, Removal of organic dyes in environmental water onto magnetic-sulfonic graphene nanocomposite, CLEAN—Soil, Air, Water 41 (2013) 992–1001.
[53] F. An, B. Gao, X. Dai, M. Wang, X. Wang, Efficient removal of heavy metal ions from aqueous solution using salicylic acid type chelate adsorbent, J. Hazard. Mater. 192 (2011) 956–962.
[54] J. Wang, S. Zheng, Y. Shao, J. Liu, Z. Xu, D. Zhu, Amino-functionalized Fe_3O_4@SiO_2 core–shell magnetic nanomaterial as a novel adsorbent for aqueous heavy metals removal, J. Colloid Interface Sci. 349 (2010) 293–299.
[55] M. Anbia, S.A. Hariri, Removal of Methylene Blue from aqueous solution using nanoporous SBA-3, Desalination 261 (2010) 61–66.
[56] M. Anbia, S.A. Hariri, S.N. Ashrafizadeh, Adsorptive removal of anionic dyes by modified nanoporous silica SBA-3, Appl. Surf. Sci. 256 (2010) 3228–3233.
[57] Y.R. Zhang, S.L. Shen, S.Q. Wang, J. Huang, P. Su, Q.R. Wang, B.X. Zhao, A dual function magnetic nanomaterial modified with lysine for removal of organic dyes from water solution, Chem. Eng. J. 239 (2014) 250–256.